Effect of the stray field of Fe/Fe 3 O 4 nanoparticles on the surface of the CoFeB thin films

R. Morgunov, O. V Koplak, R S Allayarov, E I Kunitsyna, S. Mangin

▶ **To cite this version:**

R. Morgunov, O. V Koplak, R S Allayarov, E I Kunitsyna, S. Mangin. Effect of the stray field of Fe/Fe 3 O 4 nanoparticles on the surface of the CoFeB thin films. Applied Surface Science, 2020, 527, 10.1016/j.apsusc.2020.146836 . hal-02871087v2

HAL Id: hal-02871087
https://hal.univ-lorraine.fr/hal-02871087v2

Submitted on 9 Jul 2020

HAL is a multi-disciplinary open access archive for the deposit and dissemination of scientific research documents, whether they are published or not. The documents may come from teaching and research institutions in France or abroad, or from public or private research centers.

L'archive ouverte pluridisciplinaire **HAL**, est destinée au dépôt et à la diffusion de documents scientifiques de niveau recherche, publiés ou non, émanant des établissements d'enseignement et de recherche français ou étrangers, des laboratoires publics ou privés.

Effect of the stray field of Fe/Fe_3O_4 nanoparticles on the surface of the CoFeB thin films

R. B. Morgunov[1,2,*], O. V. Koplak[1], R.S. Allayarov[1], E.I. Kunitsyna[1], S. Mangin[3]

[1]*Institute of Problems of Chemical Physics, 142432, Chernogolovka, Russia*

[2]*I.M. Sechenov First Moscow State Medical University, 119991 Moscow, Russia*

[3] *Institute Jean Lamour, UMR 7198 CNRS, Université de Lorraine, 54011 Nancy, France*

[*]morgunov2005@yandex.ru

Fe/Fe_3O_4 nanoparticles have been deposited on the surfaces of ultrathin CoFeB film and CoFeB/Ta/CoFeB hetero-structure to be detected due to the stray field generated by one particle or a cluster of particles. Exchange biased Fe/Fe_3O_4 core-shell nanoparticles have been used to stabilize the particles magnetization. Comparison between the Atomic Force and Magnetic Force Microscope images and subtraction of corresponding phase contrasts allows visualization of the film magnetization affected by the particles. Spectra of Ferromagnetic Resonance of the ultrathin films with deposited particles allow one to estimate particle/film dipolar interaction. The results will be useful for the development of lab-on-chip sensors of magnetically labeled cells. Estimation of particles number by magnetic response of the CoFeB heterostructure is demonstrated.

Key words: nanoparticles, magnetoresistive sensors, heterostructures, surface, magnetic image, ferromagnetic resonance

1. Introduction

Rapid development of giant magnetoresistance (GMR) sensors for registration, counting and selection of magnetically labeled living cells macromolecules became possible thanks to enhancement of sensors sensibility [1]. Magnetosensorics contributes to functionalizing of the nanoparticles (NP's) used for the labeling [2], new methods of magnetically driven particle displacement (magnetophoresis) [3] and microfluidic technique [4]. Fine tuning of the biomolecular recognition, quantitative treatment of information and control over sorting of groups of the biologic objects are interdependent problems, directly controlled by sensor surface properties [5-8]. Magnetoresistive sensors are usually heterostructures, sensitive to the magnetic dipole fields of NP's. Many research works were devoted to improving the sensitivity and linearity of the current. Full study of the effect of the local field generated by a single particle on the GMR structure is very important [2, 9, 10]. The creation of a magnetized area under the action of a point magnetic dipole was theoretically considered to describe the effect of magnetic cantilever on the surface of magnetic films [11-13]. Theoretical estimations were obtained for films with "in-plane" magnetization [11-13], while the films and heterostructures with perpendicular anisotropy, studied in this work, can be more effective for NP's sensors. Atomic Force Microscope (AFM) and Magnetic Force Microscope (MFM) technique allow direct visualization of the film area, which magnetization is affected by the stray field of the single ferromagnetic nano- and microparticles.

The efficiency of the NP's detection by the sensor surface depends on type and the characteristics of the NP's used as magnetic labels [14, 15]. The characteristics are the ratio between the coercive field of the particle and the coercive field of the magnetic film, the exchange bias in NP's, type and the direction of magnetic anisotropy axis. The new trend in development of the lab-on-chip GMR sensors is the use of exchange biased NP's, demonstrating high temperature stability and reversible initial state, necessary for good reproducibility [16, 17]. The core-shell NP's with the iron core and oxide shell (Fe_3O_4 and γ-Fe_2O_3) are very promising in biology application due to low chemical activity of the oxide shell and correspondent high biocompatibility [18, 19].

The goal of this paper is to study the magnetic responses of MgO/CoFeB/Ta/CoFeB/MgO/GaAs and MgO/CoFeB/Ta/MgO thin film structures with perpendicular anisotropy after deposition of Fe/Fe_3O_4 nanoparticles on their surface. More precisely we studied the magnetization reversal of these thin film structures caused by the particle stray field

2. Experimental techniques and samples

Two types of the 3 × 4.5 mm^2 samples are used: MgO (2.5nm)/CoFeB(1.1 nm)/Ta(0.75 nm)/CoFeB(0.8 nm)/MgO(2.5 nm) heterostructure (sample **I** sketched in Figure 1) and MgO(2.5

nm)/Ta(0.75 nm)/CoFeB(0.8 nm)/MgO(2.5 nm) thin film (sample **II**). These samples with perpendicular anisotropy are grown by magnetron sputtering on GaAs substrate. The structural and magnetic properties of CoFeB/Ta/CoFeB samples were determined by electron microscopy, Superconducting Quantum Interference Device (SQUID) and Magneto-Optic Kerr Effect (MOKE) techniques and are described in details in ref [20, 21]. The thicknesses of the CoFeB layers in the samples were analyzed by TEM image and EDX profile of the sample cross-section [21].

Commercially manufactured Fe/Fe_3O_4 nanoparticles were synthesized and preliminary analyzed in National University of Science and Technology MISIS (Moscow). The core/shell Fe/Fe_3O_4 NP's are grown by high temperature decomposition of the oleate iron complexes in squalene. Techniques of the nanoparticle preparation and their magnetic properties are described in [22]. Deposition of the particles on Si wafer or magnetic surfaces of CoFeB heterostructures is realized by dissolving the NP's in dimethylformamide, and then decoupling them using ultrasound bath. The concentration was ~ 1 mg/ml. The liquid of 0.1 ml volume was deposited on the surfaces of the samples preliminary cleaned in acetone (sketch of single NP on the sample **I** surface is shown in Figure 1). After drying, the particles are attached to the sample surface and allow one to mount the sample in an FMR spectrometer or a SQUID magnetometer for measurements.

Surface topography and distribution of the magnetic force gradient along the sample surface were recorded by Integra -Aura (NT MDT) atomic and magnetic force microscope. Two-pass tapping-lift algorithm of the MFM scanning provided minimization of the influence of the topography. We used standard silicon based MFM LM cantilever, covered with thin CoCr film with 400 Oe coercivity, exceeding, both, the switching fields of the thin films and NP's coercivity at room temperature. Thus, although the magnetic cantilever can affect the film magnetization, this influence is always the same and the magnetization of the cantilever tip could not be reversed. The force constant and the resonant frequency of the cantilever are 5 N/m и 63 kHz, respectively. The distance between the magnetic cantilever and the sample surface is 50 nm in MFM mode in most experiments.

The following protocol of AFM/MFM measurements was used. On the first pass, the cantilever worked in the tapping mode at the constant amplitude. In this mode, the size of the particle was determined with accuracy close to the Van der Waals radius, i.e. the distance between the cantilever and the particle was close to the cantilever oscillation amplitude. In the second pass, the cantilever was distanced from the platform surface by h =50 nm distance. The phase shift was measured at constant amplitude of the cantilever oscillations. The phase shift was directly proportional to the gradient of the magnetic dipole force between the particle and the cantilever. Revealing of the magnetized area and exceeding of its size over the particle size require obtaining the particle profile in the AFM and MFM modes in the same units. A calibration measurement was

made in which the particle size in the AFM mode (in nm) was compared with the phase contrast in the same mode (in degrees). As a result, a transition coefficient (nm to degrees) was obtained. This coefficient was chosen so that, in the absence of a magnetic substrate, the AFM and MFM size of phase contrast, expressed in degrees, coincided. This approach is applicable, if the amplitude-frequency and phase-frequency dependences of the cantilever-sample system have constant slopes in the experiments. This condition was specially tested in a separate series of experiments.

The size of the magnetic image turns out to be contingent, depending on the distance between the cantilever and the particle. The closer the cantilever to the particle, the larger the region in which the sensitivity of the device is sufficient to detect a force gradient, and the larger the MFM image of the particle. Therefore, in our experiments, the value of this distance of 50 nm was chosen so that the MFM size of the particle on the silicon substrate coincided with its AFM size. This technique was convenient because any changes in the magnetization of the film-particle system with this setting would be considered as a deviation from the zero level specified by a particle that does not interact with the substrate.

The contrast of the magnetic force image for low-coercive ferromagnetic and superparamagnetic nanoparticles can depend on the magnetization reversal of the particle by the cantilever field. This circumstance complicates the analysis and interpretation of the MFM measurement. To minimize this effect, we selected a probe with a low magnetic moment of the tip. Of course, this did not completely exclude the effect of the magnetization reversal of a particle on its size during MSM measurements; however, we assumed that this effect was the same in experiments with silicon and magnetic platforms, where the particles were deposited. The constancy of the power microscope settings in the reference experiments on silicon wafer and in the experiments on magnetic platforms made it possible to regard the deviations of the MFM profile from the reference value as evidence of the magnetization reversal of the film area around the particle.

Spectra of ferromagnetic resonance are recorded in Bruker ESP 300 *X*-band spectrometer at microwave frequency 9.880 GHz, microwave power 19.71 mW, modulation amplitude 10 Oe, modulation frequency 100 kHz. The quality factor of the microwave cavity was 5000. Field and temperature dependences of the magnetic moment were recorded by SQUID MPMS 5XL Quantum Design magnetometer in the temperature range 2 – 300 K.

3. Experimental results

3.1. Atomic and Magnetic force microscopy

The AFM and MFM two pass scanning allowed us to distinguish single Fe/Fe_3O_4 nanoparticles as well as a cluster of particles on Si substrate (Figures 2 a, b). Histogram of the particle diameters distribution, determined in the AFM mode, is shown in Figure 2 c. The average diameter of the particles is around 140 nm which corresponds to a group of nanoparticles. Indeed NP original diameter is 50 nm with very narrow distribution. Thus, ultrasound treatment does not fully separate NP's. A total of $N \approx 1.2\ 10^8$ particles of different sizes (including NP's clusters) are deposited on rectangular sample of $3 \times 4.5\ mm^2$ size in each experiment. These magnetic particles cover about 15% of the full surface.

Although we used phase shift for AFM and MFM images, we cannot compare the particle sizes given by the AFM and the MFM images directly. Indeed AFM image give the particle topography with a 0.1 – 1 nm accuracy (length of the short-ranged intermolecular forces [23]), while the MFM image is given by both the topography and the long-ranged magnetic dipolar interaction. As an example Figure 2d shows the profile given by AFM and MFM for particles deposited on diamagnetic Si. In this reference experiment, there are no magnetic forces between the substrate surface and the NP's.

Deposition of the NP's on the surface of the thin 0.8 nm CoFeB layer and the CoFeB/Ta/CoFeB heterostructure is done in a similar way. The AFM and MFM scanning results are shown in Figures 3 a and 3 b respectively. The subtraction of the MFM and AFM images reveals the magnetic part (Figure 3 c). The AFM and MFM profiles of a particle deposited on CoFeB/Ta/CoFeB platform surface are shown in Figure 3 d. The difference between the two AFM phase and MFM phase reveals the effect induced by the particle on the CoFeB magnetization.

The effect of the size of the NP's cluster array on magnetic images (magnetic halo) has been studied. First of all, the reference experiment with the NP's cluster deposited on Si diamagnetic substrate was fulfilled. Plot of the diameter of MFM phase contrast D_{MFM} versus the diameter of AFM phase contrast D_{AFM} is presented in Figure 4 (closed grey symbols). Full coincidence of the AFM and MFM image was observed for particles diameter in the 100–200 nm range. When clusters of NP's was deposited on CoFeB (open symbols in Figure 4) and CoFeB/Ta/CoFeB (full black symbols in Figure 4) samples, the MFM diameter determined experimentally always exceeded the corresponding AFM diameter. An extra halo exceeding error bar was observed for the clusters larger than 125 nm (full black symbol in Figure 4). Series of similar images demonstrating good reproducibility are shown in Supplementary section, Figure S1.

To determine the magnetic moment of the single NP's microbead, we used a method proposed in [24]. As shown in [25], shift of the cantilever frequency Δf in the MFM mode can be used to measure magnetic moment of the NP's. The Δf value depends on the magnetic moment of the individual particle $m_1 = M_S \pi 6^{-1} D_1^3$ where D_1 and M_S are the diameter and the saturated magnetization of the particle [24]:

$$\Delta f = m_1 c(h)^{-1} = M_S \pi D_1^3 \left(6c(h)\right)^{-1} \quad (1)$$

Where coefficient $c(h)$ is dependent on the lift (height) value h and the individual geometry of each cantilever. Formula (1) can be used for single domain particle mounted in the stray field of cantilever tip perpendicular to the scanning plane. Thus, each specific cantilever should be characterized by its own $c(h)$. Examples of the frequency profiles obtained for a 146 nm diameter single particle at a height value h = 50 nm is presented in Figure 5. Similar dependences of the frequency shift Δf on coordinate x were recorded at the different height values (Figure S2 a in Supplementary section**)**. Approximation of the dependence of cantilever frequency Δf on horizontal shift along OX axis by parabola gives maximal frequency shift Δf_{max} = 0.22 Hz, characterizing analyzed particle (solid line in Figure 5). Symmetry of the $\Delta f(x)$ dependence confirms the perpendicular orientation of magnetic field generated by the cantilever tip on the sample plane and the absence of the effects of the tip stray field on NP's magnetization. We used commercial product 50 nm α-Fe_2O_3 NP's with known properties as reference sample to determine constant $c(h = 50\ \text{nm}) = 1.4 \cdot 10^{-15}$ A·m^2/Hz. The value of coefficient $c(h)$ was determined for different height h accordingly to [24, 25]. Linearity of the $c(h)$ dependence (Figure 6) confirms correctness of the formula (1).

The magnetic moment of the probe 146 nm diameter Fe/Fe_3O_4 particle (Figure 2) on Si substrate was determined $m_1 = \Delta f \cdot c(h = 50\ \text{nm}) = 308$ A·nm^2 in accord with the saturated magnetization $M_S \approx 32$ A · m^2/kg, independently determined by SQUID magnetometer (see next section 3.2).

Similar dependences of the phase shift $\Delta\varphi$ on coordinate x were recorded at the different height values (Figure S2 b in Supplementary section**)**. We found, that the phase shift is given by

$$\Delta\varphi = f_0 m_1 c(h)^{-1} = f_0 M_S \pi D_1^3 \left(6c(h)\right)^{-1} \quad (2)$$

where f_0 is a constant. Thus, we have to conclude, that phase analysis of the MFM and AFM images is valid to determine particle magnetic moment as well as frequency analysis of the cantilever oscillations. The linear dependence of $c(h)$ allows to extract MFM and AFM phase contrasts for different particles size.

3.2. Magnetic hysteresis loop of the thin films with deposited nanoparticles

The goal of this section is to determine using magnetization measurements the effect of the presence of Fe/Fe_3O_4 nanoparticles on the different samples. Magnetization as a function applied magnetic field $M(H)$ of the CoFeB thin film (loops **1** in Figures 7 a) and the CoFeB/Ta/CoFeB heterostructure (loops **1** in Figures 7 b) whithout any NPs are recorded by SQUID magnetometer at three different temperatures 300 K, 100 K and 2 K. Similar M(H) measurements were performed for NP's deposited on a Si substrate (loops **2** in Figures 7 a, b) and on single CoFeB layer and CoFeB/Ta/CoFeB (loops **3** in Figures 7 a and 7 b, respectively). In the case of CoFeB/Ta/CoFeB structure, four stable magnetic states can be accessed two stable 'parallel' states (P^+, P^-) and two 'antiparallel' (AP^+ and AP^-) states correspond to the four levels observed in the $M(H)$ curves. The P^+ state corresponds to a parallel alignment of the magnetizations of the thick and thin layers along the external magnetic field (↑↑), P^- state corresponds to both layers magnetized opposite to the field (↓↓), and two phases AP^+ and AP^- correspond to an inverse directions of the two layers magnetization (↑↓) and (↓↑),.

The solid orange lines covering blue symbols in loops **3** Figures 7 a for the monolayer and Figure 7 b for the bilayer correspond to the sum of the separately measured magnetic field dependences for the films without NPs (sample **I** or **II**) and the NP's on Si substrate. One can see an excellent correspondence between the solid orange line with the blue experimental points at 100 K and 300 K. The solid orange line differs from the blue dots only at 2K for applied magnetic field exceeding 300 Oe (Figure 7 b). One can observe small change in the saturated magnetization by ~ 0.1 emu in monolayer and bilayer and small change of the switching critical field in bilayer by ~ ΔH_C = 50–70 Oe at low temperature. Similar effects were described and discussed early in [25], for the deposition of the α-Fe_2O_3 NP's on the same single layer and multilayers.

Field dependence of the magnetization of Fe/Fe_3O_4 nanoparticles deposited on silicon wafer is similar than the one obtained for an assembly of superparamagnetic particles. In case of an isotropic assembly, the field dependence of the total magnetization (Figure 8) can be described by Langevin function [27]:

$$M(H) = M_S^{SPM}\left[\coth\left(\frac{\mu_0 mH}{k_B T}\right) + \left(\frac{\mu_0 mH}{k_B T}\right)^{-1}\right] + C^{PM} H \qquad (3)$$

μ_0 is the vacuum permeability, M_S^{SPM} is the average projection of the magnetic moment along the field direction, m is average magnetic moment of each NP's cluster, $M_S^{SPM} = mN$ is saturation magnetization, N is number of particles, k_B is Boltzman constant, T is temperature, C^{PM} is magnetic susceptibility of paramagnetic contribution, appearing due to impurities in Si substrate. Using expression (3) gives an average magnetic moment $m = 28.5 \cdot 10^{-14}$ emu = $28.7 \cdot 10^{-17}$ A·m^2 = 287

A·nm^2 for an average diameter D = 140 nm. These estimations are in good agreement with the data obtained by MFM technique (m_1 = 308 A·nm^2 at AFM determined diameter D_1 = 146 nm).

3.3. Effect of the nanoparticles on ferromagnetic resonance of the thin films

Ferromagnetic resonance (FMR) spectrum is sensitive to particle-film interaction as shown below. Comparison of the single FMR spectra, recorded before and after deposition of the NP's on the sample **II** can lead to wrong conclusions due to non controllable orientation of the sample in microwave cavity, determined with 10 degree accuracy. To minimize this issue we recorded systematical series of the FMR spectra at different angles θ between magnetic field orientation and the film normal (Figure 9).

Figure 9 a shows the FMR spectra at 300 K for sample **II** (single CoFeB layer) without any NP in the angle range θ = 0 – 180 degree, which were recorded with 5 degree step. Anisotropic line **A** and isotropic line **B** are centered at about H_{RES} ~ 3 kOe and described in [28].

The FMR spectrum of the NP's clusters on silicon diamagnetic wafer contains two isotropic lines (Supplementary section Figure S3). This FMR spectrum is well known for the Fe/Fe_3O_4 NP's and it was described in [29]. Low field line corresponds to the NP's with easy axis perpendicular to external field, while high field line corresponds to the NP's aligned along field direction.

Series of FMR spectra of the sample **II** with deposited NP's clusters for different θ = 0 – 180 degree is shown in Figure 9 b. There are four lines **A**, **B**, **C**, **D**, observed in the spectra (Figure 9 b). In case of NP clusters on CoFeB film without any interaction, one can expect four lines due to the summation of the two lines of FMR spectra of the CoFeB platform and the two lines of the NP's clusters. Obvious change can be observed, the two resonant lines **C** and **D** belonging to NP's show angle dependence, i.e. their resonant field becomes sensitive to orientation of the sample **II** with deposited NP's in respect to external magnetic field (Figure 9 b). One can conclude that the anisotropy observed for lines **C** and **D** are due to the dipolar interaction between NP's and ferromagnetic surface of CoFeB film. Amplitude of angular dependence $\Delta H_{RES} \approx 450$ Oe of the line **C** of NP's corresponds to the additional field acting on NP's cluster from magnetic surface. This gives opportunity to estimate an average energy of the magnetic dipole interaction $E_{dip} = m\,\Delta H_{RES} = 1.3\ 10^{-10}$ erg, m is average magnetic moment of NP's cluster.

Comparison of the FMR spectrum of CoFeB film without NP's, FMR spectrum of NP's deposited on Si wafer and their sum with the experimental FMR spectrum of CoFeB film with deposited NP's are shown in Supplementary section, Figure S4 for selected angles θ = 0º, 45º, 90º. This comparison allows one to conclude, that the shift of the **A** and **B** lines of the CoFeB film

appears under the magnetic stray field of the magnetic particles deposited on surface. Thus, FMR technique allows one to observe, both, the effect of NP's clusters on CoFeB spectrum and the influence of the CoFeB on the NP's spectrum. The same conclusions can be obtained from the comparison of the dependences of the resonant field H_{RES} on the angle θ for lines **A** and **B** in CoFeB film without NP's with the correspondent lines **A** and **B** in CoFeB film with deposited NP's. The lines **C** and **D** of NP's deposited on CoFeB film becomes anisotropic in comparison with the initial isotropic lines **C**, and **D** of NP's deposited on Si wafer (Figure 10).

Thus, FMR spectra are very sensitive to the dipolar interaction between the CoFeB film and NP's clusters. Shift of the resonant field for CoFeB as well as shift of the resonant field for NP's and resonant field anisotropy can be used to estimate the average value of the dipolar interaction. The spin dynamics in CoFeB films and in the Fe/Fe_3O_4 nanoparticles is controlled by exchange interaction, magnetic anisotropy and external magnetic fields including demagnetizing field of the nanoparticles. Damping factors corresponding to energy dissipation control over the decay of spin precession and additionally contribute to the spin dynamics. All mentioned above interactions effect shape and main parameters of the FMR lines (resonant field and linewidth) accordingly to the Landau-Lifshitz-Hilbert equation. Deposition of the particles on ferromagnetic surface of the ferromagnetic film accompanies with the appearing of the magnetic dipole interaction between ferromagnetic film and nanoparticles. All the rest mentioned above factors of spin dynamics do not change after the particles deposition. Magnetic dipole interaction in system particle-film changes effective magnetic field providing spin precession in the both systems. For that reason the resonant frequency of FMR signals of the nanoparticles and thin film were changed in our experiments. Since magnetic dipole interaction possesses an axial symmetry with the axis along particle- surface normal, anisotropy of the resonant shift appears in the particle-film system. This circumstance explains, why the resonant fields of the initially isotropic lines **C** and **D** belonging to nanoparticles (Figure 9a) becomes anisotropic after the particles deposition (Figure 9b). The shift of the resonant lines **A** and **B** belonging to the ferromagnetic film is obviously caused by additional field of nanoparticles summing with the external field of the spectrometer. The analogous effect can be expected for double layered sample **I**, when nanoparticle deposited on its surface.

4. Discussion

In our experiments AFM and MFM images were recorded for the same individual particle (or clusters of NP's array) and treated by Gwyddion software to obtain corresponding AFM and MFM profiles. Nanoparticles diameter obtained by MFM (D_{MFM}) and by AFM (D_{AFM}) are found to be different because of the interaction between the magnetic film and the NP . A simple model is developed to describe magnetization reversal of the film under the NP's clusters. NP's clusters are described as balls possessing a magnetic dipole in their centers. Below NP's one can expect formation of the P^- phase with magnetic moments of the CoFeB layers directed along NP's stray field in the same direction (↓↓) (Figure 1). Far from the NP's cluster the initial AP^+ state of the spin valve (↑↓) should be observed, because of the antiferromagnetic exchange between the CoFeB layers. Radius of the P^- area R_1, radius of the AP^- area R_2, altitude of NP's cluster center k above sample surface and radius of NP's cluster R are shown in Figure 1.

The P^-, AP^- and AP^+ areas are shown in Figure 11, together with the correspondent energy diagrams calculated by minimization of the local energy of the spin valve depending on Θ_1 (angle between the upper CoFeB layer magnetization and the perpendicular axis Oz) and Θ_2 (angle between the lower CoFeB layer magnetization and the perpendicular axis Oz).Similar calculations were performed in ref [21]. Local energy density of the spin valve CoFeB/Ta/CoFeB can be presented as sum of anisotropy energy of layers E_{aniz}, Zeeman energy E_{Zeem} and exchange energy E_{ex}. These terms can be presented as:

$$E_{aniz}(\Theta_1, K_{S1}, \Theta_2, K_{S2}) = -K_{S1}\cos(\Theta_1)^2 - K_{S2}\cos(\Theta_2)^2$$
$$E_{Zeem}(t_1, H, \Theta_1, M_{S1}, t_2, M_{S2}, \Theta_2) = -\mu H(t_1 M_{S1}\cos(\Theta_1) + t_2 M_{S2}\cos(\Theta_2))$$
$$E_{ex}(J_{af}, \Theta_1, \Theta_2) = -J_{af}\cos(\Theta_1 - \Theta_2) \qquad (4)$$

t_1 and t_2 are thicknesses of the upper and bottom layers correspondently, M_{S1} and M_{S2} are their saturation magnetizations, K_{S1} and K_{S2} are constants of magnetic anisotropy of the correspondent CoFeB layers, J_{af} is interlayer exchange constant. Examples of minimization of the sum $E = E_{aniz} + E_{Zeem} + E_{ex}$ performed with the Wolfram Mathematica software are presented in the insertions in Figure 11. We used t_1, t_2, M_{S1}, M_{S2}, K_{S1}, K_{S2}, J_{af} parameters early determined in [26].

Switching between P^-, AP^- and AP^+ stable states requires perpendicular component of external critical field H_1 = -20 Oe for the $AP^+ \rightarrow AP^-$ transition and H_2 = -240 Oe for the $AP^- \rightarrow P^-$ transition (these critical fields were experimentally determined from magnetic hysteresis loop of the sample **I**). We used formula of point magnetic dipole to calculate perpendicular component of the magnetic field in current point of the spin-valve surface:

$$H_Z(p_m, r, k) = \frac{1}{4\pi}\left[\frac{-p_m}{(r^2+k^2)^{1.5}} + \frac{3p_m k^2}{(r^2+k^2)^{2.5}}\right] \qquad (5)$$

p_m is the projection of magnetic moment on the *OZ* axis, *r* is horizontal distance between projection of the NP's center on CoFeB plane and current point, *k* is altitude of the magnetic NP's over the sample plane, due to the capping r layer and the organic substrate always separating NP's from sample surface. The *k* value includes NP's radius $R=D/2$ and h_{add}, additional thickness of the layer between sample surface and magnetic nanoparticles (see Figure 1).

The equations describing radiuses R_1 and R_2 of the magnetically reversed areas (Figure 1) are obtained from the condition, one the critical fields H_1 and H_2, respectively:

$$H_Z(p_m, R_1, k) = H_1 \quad (6),$$

$$H_Z(p_m, R_2, k) = H_2 \quad (7),$$

These equations can be expressed by formula:

$$\frac{p_m^A R^3}{4\pi R_A^3 (r^2 + (R + h_{add})^2)^{2.5}} \left\{2(R + h_{add})^2 - r^2\right\} = H_C \quad (8)$$

The average magnetic moment of the NP's cluster p_m^A = -287 A nm^2, and the average particle radius $R = R_A$ = 70 nm with $H_C = H_1$ = -20 Oe and $H_C = H_2$ = -240 Oe allows to obtain $R_{MFM}(R_{AFM})$ and $D_{MFM}(D_{AFM})$ dependences using equation (8).

In Figure 4, the solid line **1** shows the dependence of the MFM size on the AFM size for NP's deposited on Si substrate. Line **2** is $D_{MFM}(D_{AFM})$ dependence, calculated for AP$^-$ phase in CoFeB/Ta/CoFeB platform with the h_{add} = 66 nm gap between the NP's and the surface. If we calculate $D_{MFM}(D_{AFM})$ dependence with h_{add} = 0, the size of magnetic image of the AP$^-$ phase is larger, than it was observed in our experiments (line **3** in Figure 4). The size of the P$^-$ magnetic phase is always smaller, than NP's size (line **4** in Figure 4). Thus, P$^-$ magnetic phase is always covered by NP's cluster and cannot be observed by MFM techniques. We can conclude, that we could only observed AP$^-$ phase in our experiments because to its large size.

The proposed model is very simple and does not take into account many factors such as the demagnetizing field of the magnetic domains and the domain walls energies which play an important for small areas with diameter below 10 – 100 nm. We neither considered magnetic field of cantilever tip, which influence is described in [11]. We assumed a ball shape of the NP's clusters, while real shape can be different and we neglected that the NP's magnetization could reverse. This effect is definitely exists and revealed experimentally by FMR technique (see Figure 9).

We used OOMMF (the Object Oriented Micro Magnetic Framework) software [30] for micromagnetic modeling of the spin valve with the perpendicular anisotropy. We performed the calculation using a 700 × 700 nm area with 5 × 5 nm unit cell. Magnitude and direction of

magnetization was determined for each cell. Anisotropy constants K_{S1} = 2.5 10^{-3}erg/cm^2 and K_{S2} = 4 10^{-3}erg/cm^2 for upper and bottom layers respectively, interlayer exchange constant J_{af} = -10^{-2} erg/cm^2, intralayer exchange constant J_{ex} = 10^{-6} erg/cm, saturation magnetizations M_{S1} = 952 emu/cm^3 and M_{S2} = 1040 emu/cm^3, early determined in [28] was used. The applied homogeneous magnetic field, is replaced by the magnetic field from the dipole given by (5). The initial configuration of the spin valve is the AP$^+$ one, corresponding to zero external magnetic field. In Figure 12 a, b, results of calculations are shown for a 100 nm radius particle deposited on the CoFeB/Ta/CoFeB surface.

Similar calculation of the magnetically reversed area 700 nm × 700 nm was performed for the single layer (Figure 12 c) with the following parameters J_{ex} = 10^{-6} erg/cm, saturation magnetizations M_{S1} = 952 emu/cm^3, K_1 = 2.5 · 10^{-3}erg/cm^2.

One can conclude that the reversed area, predicted by micromagnetic simulation, is larger, than the geometrical size of the NP's cluster scanned by AFM for both, spin valve surface and single layer. In case of homogeneous particles in terms of size, we will observe magnetically reversed areas with the size exceeding particle starting from ~ 100 nm diameters. Tuning of the particle type or ferromagnetic platform type can change this threshold value. In case of the spin valve, the radius of magnetically reversed area is smaller, that for the monolayer, because interlayer antiferromagnetic interaction tend to avoid magnetization reversal. Directly under the NP's cluster one can observe disc area corresponding to the P$^-$ phase. The radius of this area is always shorter, than the NP's radius. One can conclude, that P$^-$ phase under NP's cannot be detected, because it is always covered by the NP's. There is ~ 100 nm wide transition area (ring of light color) in between P$^-$ and AP$^+$ areas. This area with spins oriented in-plane strongly depends on the H_X component of the dipolar field. This component overcomes magnetic anisotropy and aligns spins in CoFeB plane. The area far from the dipole > 200 nm corresponds to the initial AP$^+$ state of the bilayer or of the monolayer as expected because of the value of the field lower than the switching value.

Conclusions

1. The size of Fe/Fe_3O_4 nanoparticles deposited on CoFeB ferromagnetic thin film given by the AFM and MFM phase contrasts was studied. Comparison between the two types of phase contrast allowed us to determine the magnetization area in the film reversed under the magnetic stray field of the ferromagnetic particle.

2. Deposition of Fe/Fe_3O_4 particle on CoFeB film and CoFeB/Ta/CoFeB bilayer causes changed in the FMR measurements performed on the magnetic films due to the local effect of

particles magnetic stray fields. Shift of the resonant fields of the Fe/Fe_3O_4 particles and magneto induced anisotropy of FMR spectrum of the nanoparticle clusters are observed

3. Theoretical estimation and OOMMF modeling of the diameter of the CoFeB film area, which magnetization is reversed under the dipolar magnetic field created by the Fe/Fe_3O_4 particle, are obtained. They are found to be in good agreements with the area observed experimentally.

4. Proof of the interaction between the magnetization of the nanoparticles and the thin film can be observed at low temperatures ~ 2 K using SQUID magnetometer.

Acknowledgments

R.M. was supported by the Russian academic excellence project “5-100" for I.M. Sechenov First Moscow State Medical University.

The work was performed in accordance with the program of Institute of Problems of Chemical Physics AAAA-A19-119092390079-8 and supported by Grant of President of Russian Federation for Scientific School 2644.2020.2. S.M. was supported by the Région Grand Est, by the Metropole Grand Nancy, by the impact project LUE-N4S, part of the French PIA project “Lorraine Université d’Excellence”, reference ANR-15IDEX-04-LUE, and by the “FEDER-FSE Lorraine et Massif Vosges 2014-2020”, a European Union Program.

References

1. D.L.Graham, H.A.Ferreira, N.Feliciano, P.P.Freitas, L.A.Clarke, M.D.Amaral, Magnetic field-assisted DNA hybridisation and simultaneous detection using micron-sized spin-valve sensors and magnetic nanoparticles, Sensors and Actuators B: Chemical, 107(2), (2005) 936-944. https://doi.org/10.1016/j.snb.2004.12.071

2. H. T. Huang, P. Garu, C. H. Li, W. C. Chang, B. W. Chen, S. Y. Sung, C. M. Lee, J. Y. Chen, T. F. Hsieh, W. J. Sheu, H. Ouyang, W. C. Wang, C. R. Chang, C. L. Wang, M. S. Hsu and Z. H. Wei, Magnetoresistive Biosensors for Direct Detection of Magnetic Nanoparticle Conjugated Biomarkers on a Chip, SPIN, 09(02) (2019), 1940002. https://doi.org/10.1142/S2010324719400022

3. N. Pamme, C. Wilhelm, Continuous sorting of magnetic cells via on-chip free-flow magnetophoresis, Lab Chip, 6 (2006) 974–980. https://doi.org/10.1039/b604542a

4. I. Giouroudi, G. Kokkinis, Recent Advances in Magnetic Microfluidic Biosensors, Nanomaterials (Basel), 7(7) (2017), 171. https://dx.doi.org/10.3390%2Fnano7070171

5. D. L. Graham, H. Ferreira, J. Bernardo, P. P. Freitas, J. M. S. Cabral, Single magnetic microsphere placement and detection on-chip using current line designs with integrated spin valve sensors: biotechnological applications, J. Appl. Phys., 91 (2002) 7786–7788. https://doi.org/10.1063/1.1451898

6. H. A. Ferreira, D. L. Graham, P. P. Freitas, J. M. S. Cabral, Biodetection using magnetically labeled biomolecules and arrays of spin valve sensors, J. Appl. Phys., 93 (2003) 7281–7286. https://doi.org/10.1063/1.1544449

7. G. Li, V. Joshi, R. L. White, S. X. Wang, Detection of single micron-sized magnetic bead and magnetic nanoparticle using spin valve sensors for biological applications, J. Appl. Phys., 93 (2003) 7557–7559. https://doi.org/10.1063/1.1540176

8. J. Schotter, P.B. Kamp, A. Becker, A. Puhler, D. Brinkmann, W. Schepper, H. Bruckl, G. Reiss, A biochip based on magnetoresistive sensors, IEEE Trans. Magn., 38 (2002) 3365–3367. https://doi.org/10.1109/TMAG.2002.802290

9. G. Li, S. X. Wang, Analytical and micromagnetic modeling for detection of a single magnetic microbead or nanobead by spin valve sensors, IEEE Trans. Magn., 39 (2003) 3313–3315. https://doi.org/10.1109/TMAG.2003.816760

10. M. Tondra, M. Porter, R. Lipert, Model for detection of immobilized superparamagnetic nanosphere assay labels using giant magnetoresistive sensors, J. Vac. Sci. Technol. A, 18 (2000) 1125–1129. https://doi.org/10.1116/1.582476

11. V. L. Mironov, A. A. Fraerman, B. A. Gribkov, O. L. Ermolayeva, A. Yu. Klimov, S. A. Gusev, I. M. Nefedov, I. A. Shereshevskii, Control of the Magnetic State of Arrays of Ferromagnetic Nanoparticles with the Aid of the Inhomogeneous Field of a Magnetic Force Microscope Probe, The Physics of Metals and Metallography, 110 (2010) 708–734. https://doi.org/10.1134/S0031918X10130053

12. V. L. Mironov, O. L. Ermolaeva, S. A. Gusev, A. Yu. Klimov, V. V. Rogov, B. A. Gribkov, O. G. Udalov, A. A. Fraerman, R. Marsh, C. Checkley, R. Shaikhaidarov, V. T. Petrashov, Antivortex State in Crosslike Nanomagnets, Phys. Rev. B, 81 (2010) 094436(1-5). https://doi.org/10.1103/PhysRevB.81.094436

13. V. L. Mironov, B. A. Gribkov, A. A. Fraerman, S. A. Gusev, S. N. Vdovichev, I. R. Karetnikova, I. M. Nefedov, I. A. Shereshevsky, MFM Probe Control of Magnetic Vortex Chirality in Elliptical Co Nanoparticles, J. Magn. Magn. Mater., 312 (2007) 153–157. https://doi.org/10.1016/j.jmmm.2006.09.032

14. G.V.M. Williams, T. Prakash, J. Kennedy, S.V.Chong, S.Rubanov, Spin-dependent tunnelling in magnetite nanoparticles, Journal of Magnetism and Magnetic Materials, 460 (2018) 229–233. https://doi.org/10.1016/j.jmmm.2018.04.017

15. J. Kennedy, J. Leveneur, G.V.M.Williams, D. R.G.Mitchell and A.Markwitz, Fabrication of surface magnetic nanoclusters using low energy ion implantation and electron beam annealing, Nanotechnology 22 (2011) 115602 (1-6). https://doi.org/10.1088/0957-4484/22/11/115602

16. V. Skumryev, S. Stoyanov, Y. Zhang, G. Hadjipanayis, D. Givord, J. Nogues, Beating the superparamagnetic limit with exchange bias, Nature, 423 (2003) 850-853. https://doi.org/10.1038/nature01687

17. Q. K. Ong, X.-M. Lin, A. Wei, The Role of Frozen Spins in the Exchange Anisotropy of Core–Shell Fe@Fe_3O_4 Nanoparticles, J. Phys. Chem. C. Nanomater Interfaces, 115(6) (2011), 2665–2672. https://dx.doi.org/10.1021%2Fjp110716g

18. D. Chen, Q. Tang, X. Li, X. Zhou, J. Zang, W.-q. Xue, J.-y. Xiang, C.-q. Guo, Biocompatibility of magnetic Fe_3O_4 nanoparticles and their cytotoxic effect on MCF-7 cells, Int. J. Nanomedicine. 7 (2012), 4973–4982. https://dx.doi.org/10.2147%2FIJN.S35140

19. G. S. Demirer, A. C. Okurb, S. Kizilel, Synthesis and design of biologically inspired biocompatible iron oxide nanoparticles for biomedical applications, J. Mater. Chem. B, 3 (2015), 7831-7849. https://doi.org/10.1039/C5TB00931F

20. O. Koplak, A. Talantsev, Y. Lu, A. Hamadeh, P. Pirro, T. Hauet, R. Morgunov, S. Mangin, Magnetization switching diagram of a perpendicular synthetic ferrimagnet CoFeB/Ta/CoFeB bilayer, Journal of Magnetism and Magnetic Materials, 433 (2017) 91-97. https://doi.org/10.1016/j.jmmm.2017.02.047

21. R. Morgunov, Y. Lu, M. Lavanant, T. Fache, X. Deveaux, S. Migot, O. Koplak, A. Talantsev, and S. Mangin, Magnetic aftereffects in CoFeB/Ta/CoFeB spin valves of large area, Physical Review B 96 (2017), 054421. https://doi.org/10.1103/PhysRevB.96.054421

22. J. Salado, M. Insausti, L. Lezama, I. Gil de Muro, E. Goikolea, T. Rojo, Preparation and Characterization of Monodisperse Fe3O4 Nanoparticles: An Electron Magnetic Resonance Study, Chem. Mater. 23 (2011), 2879–2885. https://doi.org/10.1021/cm200253k

23. F. L. Leite, C. C. Bueno, A. L. Da Róz, E. C. Ziemath, O. N. Oliveira, Theoretical Models for Surface Forces and Adhesion and Their Measurement Using Atomic Force Microscopy, International Journal of Molecular Sciences. 13(10) (2012) 12773–12856. https://doi.org/10.3390/ijms131012773

24. S. Sievers, K.-F. Braun, D. Eberbeck, S. Gustafsson, E. Olsson, H. W. Schumacher, U. Siegner, Quantitative measurement of the magnetic moment of individual magnetic nanoparticles by magnetic force microscopy, Small 8(17) (2012) 2675. https://doi.org/10.1002/smll.201200420

25. O. Koplak, O. Haziahmatova, L. Litvinova, O. Dmitriev, R. Morgunov, Effect of α-Fe2O3 microbeads on CoFeB/Ta/CoFeB magnetic switching and magnetic instabilities, Superlattices and Microstructures 121 (2018) 23-32. https://doi.org/10.1016/j.spmi.2018.07.019

26. A. Talantsev, Y. Lu, T. Fache, M. Lavanant, A. Hamadeh, A. Aristov, O. Koplak, R. Morgunov, S. Mangin, Relaxation dynamics of magnetization transitions in synthetic antiferromagnet with perpendicular anisotropy, J. Phys.: Condens. Matter, 30 (2018), 135804(1-10). https://doi.org/10.1088/1361-648X/aaaf04

27. S. Tikadzumi, Ferromagnetism nature. Magnetic characteristics and practical applications, Mir, Moscow, 1987, p 419.

28. R.B. Morgunov, G.L. L'vova, A.D. Talantsev, Y. Lu, X. Devaux, S. Migot, O.V. Koplak, O.S. Dmitriev, S. Mangin, Ferromagnetic resonance of CoFeB/Ta/CoFeB spin valves versus CoFeB film, Thin Solid Films, 640 (2017) 8-13. https://doi.org/10.1016/j.tsf.2017.08.029

29. M. M. Can, M.Coşkun, T.Fırat, A comparative study of nanosized iron oxide particles; magnetite (Fe3O4), maghemite (γ-Fe2O3) and hematite (α-Fe2O3), using ferromagnetic

resonance, Journal of Alloys and Compounds, 542 (2012), 241-247. https://doi.org/10.1016/j.jallcom.2012.07.091

30 . M.J. Donahue, D.G. Porter, OOMMF User's Guide, Version 1.0, Interagency Report NISTIR 6376, National Institute of Standards and Technology, Gaithersburg, MD, Sept. 1999. https://math.nist.gov/oommf/

Captions for figures

Figure 1. Sketch of the CoFeB/Ta/CoFeB (sample **I**) and the magnetization area reversed by the magnetic stray field generated by a single Fe/Fe_3O_4 particle

Figure 2. Images of Fe/Fe_3O_4 particles deposited on a Si surface, recorded in AFM mode (a), in MFM mode (b). Histogram of diameter of particles (D) distribution (c). Profiles of the phase contrasts recorded in AFM and MFM modes for Fe/Fe_3O_4 particles deposited on Si surface (d).

Figure 3. Images of Fe/Fe_3O_4 particles deposited on CoFeB/Ta/CoFeB surface, recorded in AFM mode (a), in MFM mode (b). Extraction of the AFM phase contrast from the MFM phase contrast (c). Profiles of the MFM and MFM phase contrasts of Fe/Fe_3O_4 particle, deposited on CoFeB/Ta/CoFeB surface (d).

Figure 4. Fe/Fe_3O_4 particle diameter obtained from MFM measurements (D_{MFM}) as a function of the diameter obtained from AFM measurements (D_{AFM}). Closed grey symbols: for particles deposited on Si substrate. open symbols for particles deposited on CoFeB thin film and closed black symbols for particles deposited on CoFeB/Ta/CoFeB multilayer. Solid lines are theoretical D_{MFM} (D_{AFM}) dependences for NP's on Si substrate (1), for NP's separated by 66 μm additional layer from CoFeB/Ta/CoFeB platform, initially presented in AP^- state (2), for NP's directly contacting with CoFeB/Ta/CoFeB platform, initially presented in AP- state (3), for NP's directly contacting with CoFeB/Ta/CoFeB platform, initially presented in P- state (4).

Figure 5. Frequency deviation Δf for MFM scanned single nanoparticles cluster of 146 nm diameter on Si wafer. The dependence was recorded at 50 nm height. Solid line is an approximation using a parabola. Dashed line corresponds to zero frequency shift.

Figure 6. Calibration factor $c(h)$ as a function of the cantilever height for NP's deposited on Si wafer. The solid line is a linear regression fit.

Figure 7. Magnetization as a function of the applied field for at 300 K, 100 K and 2 K: (a) a single CoFeB monolayer (sample **II**) (b) CoFeB/Ta/CoFeB bilayer (samples **I**) . Series **1** correspond to the samples **I** or **II** without NP's, series **2** correspond to magnetic Fe/Fe_3O_4 particles deposited on the Si

surface, series 3 correspond to samples **I** and **II** with Fe/Fe_3O_4 particles. Solid orange line is the sum of the signal obtained in series 1 and series 2.

Figure 8. Magnetisation of Fe/Fe_3O_4 nanoparticles deposited on Si wafer as a function of field at 300 K. Solid line is a fit using a Langevin function.

Figure 9. FMR spectra of sample **II** without NP's (a) and with NP's (b), recorded at different angles between the magnetic field and the direction perpendicular to the film. Positions of lines are shown by colors. Anisotropic line **A** and isotropic line **B** corresponds to the CoFeB monolayer. Lines **C** and **D** corresponds to the NP's.

Figure 10. Angle dependences of the resonant field H_{RES} for lines **A** (black symbols) and **B** (blue symbols) in sample **II** without NP's (open symbols) and with NP's (closed symbols). Lines **C** (green symbols) and **D** (orange symbols) of NP's deposited on CoFeB platform (close circles), on Si wafer (close squares).

Figure 11. Magnetization states P^-, AP^- and AP^+ of the sample **I** and correspondent energy profiles calculated in (Θ_1:Θ_2) space. The Θ_1 is angle the upper CoFeB layer magnetization and the perpendicular axis Oz) and Θ_2 (angle the lower CoFeB layer magnetization and the perpendicular axis Oz)

Figure 12. Magnetic configuration in the bottom (a) and upper (b) CoFeB layers of bilayer and monolayer (c) under the magnetic field generated by 100 nm radius NP's cluster. Red color corresponds to magnetization directed towards reader; blue color corresponds to opposite magnetization direction. Sizes of the modulated sample`s area are 700 nm × 700 nm. Solid circles correspond to real size of NP's cluster determined by AFM technique and assumed in the calculations. Arrows correspond to the projection of the magnetization in individual cells.

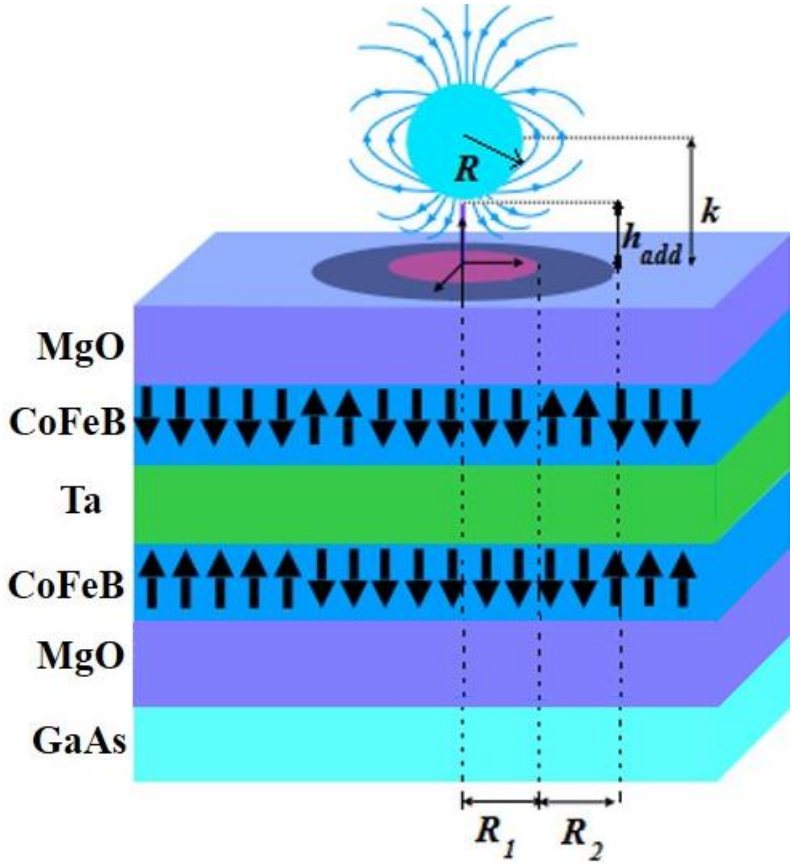

Figure 1.

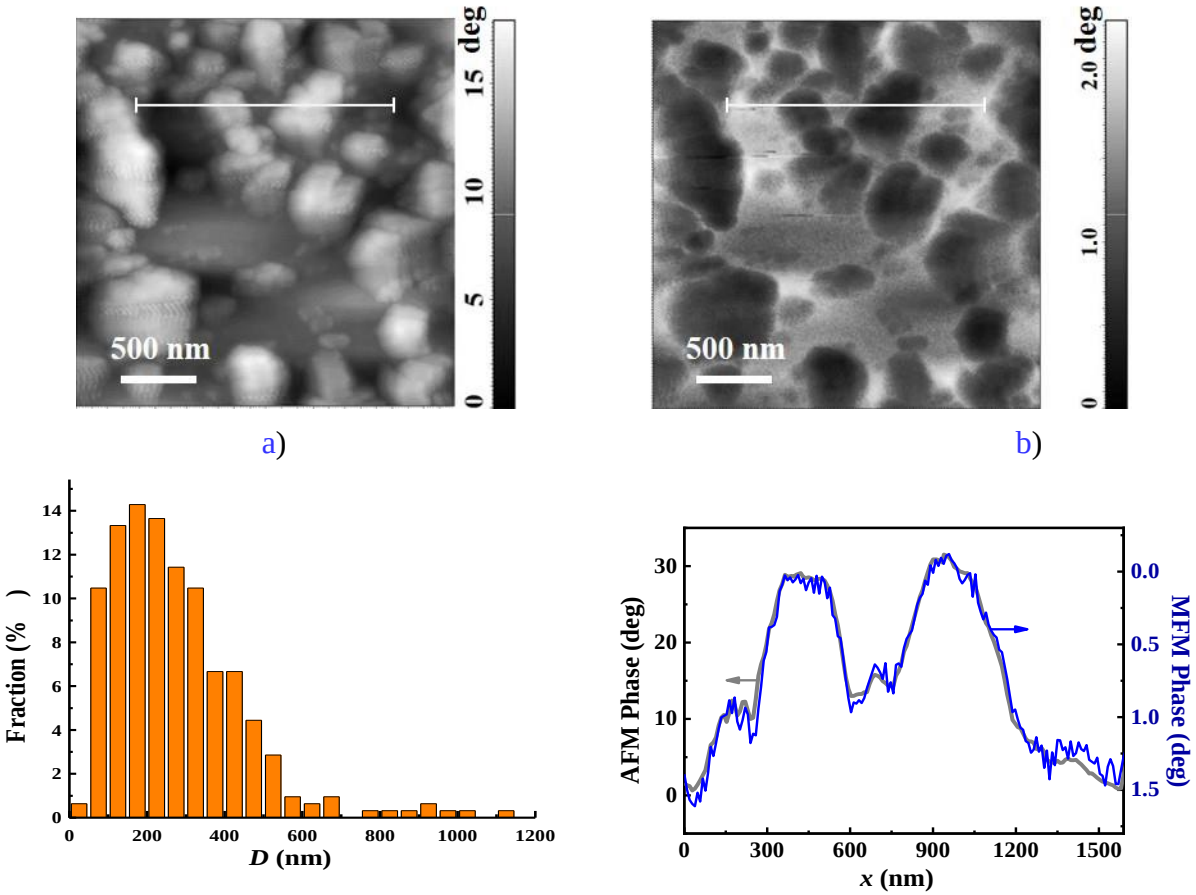
500 nm
15 deg
10
5
0
a)
500 nm
2.0 deg
1.0
0
b)
Fraction (%)
D (nm)
c)
AFM Phase (deg)
MFM Phase (deg)
x (nm)
d)

Figure 2.

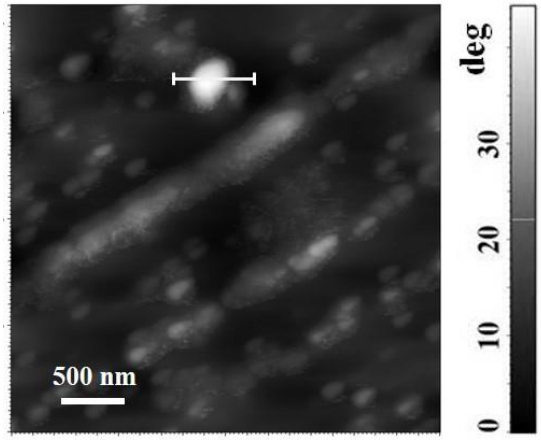

a)

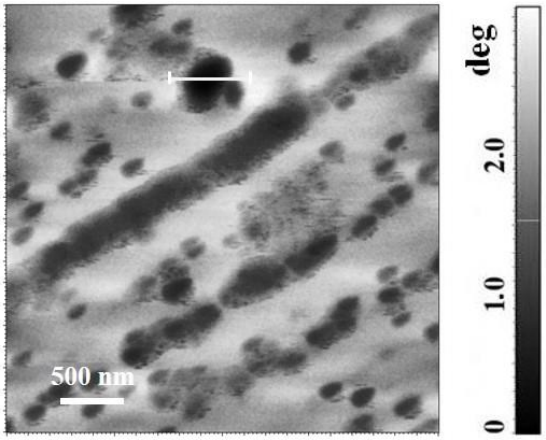

b)

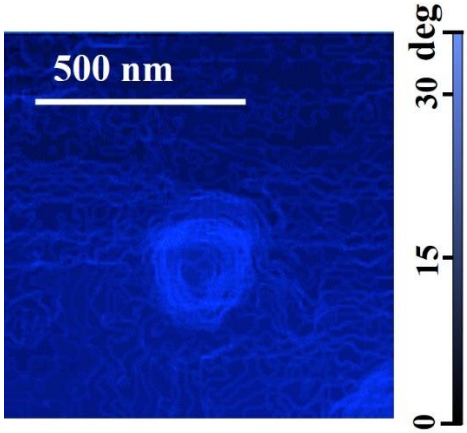

c)

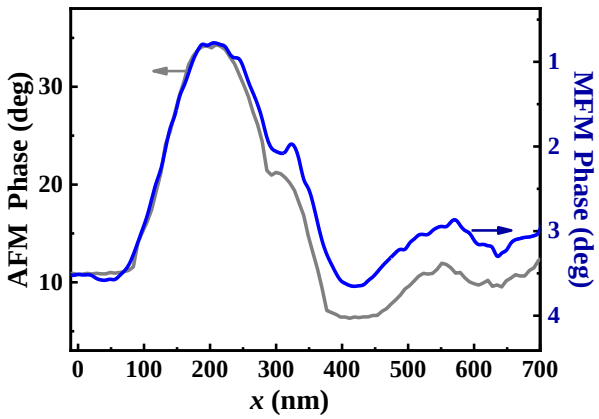

d)

Figure 3.

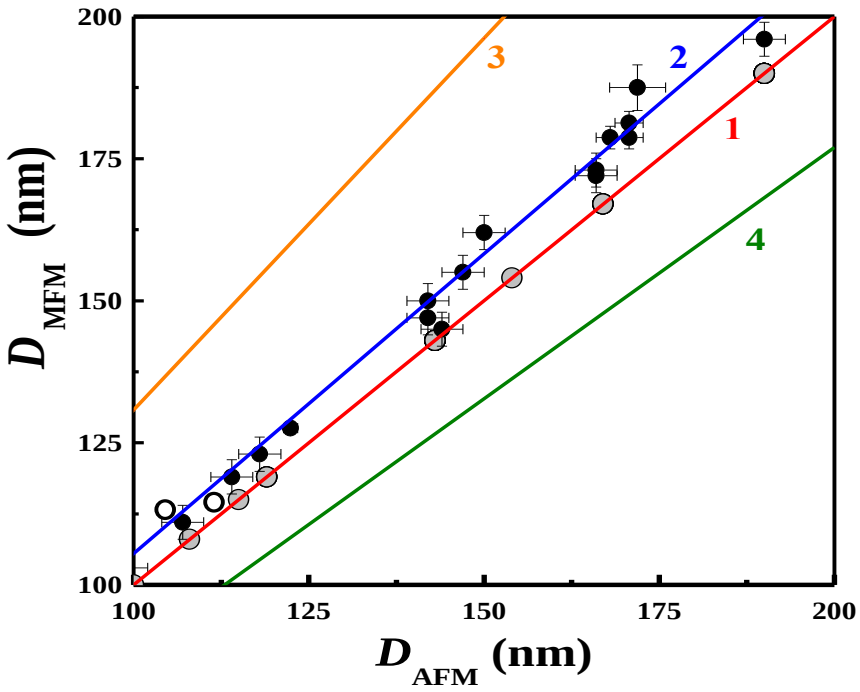

Figure 4.

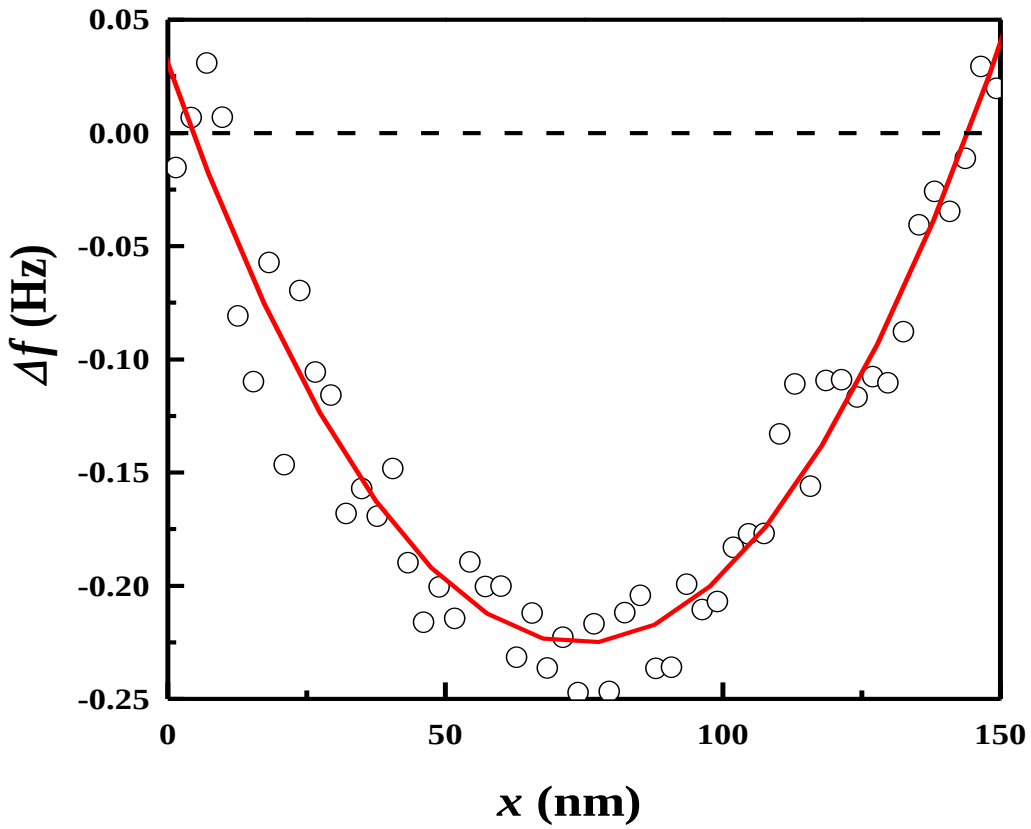

Figure 5.

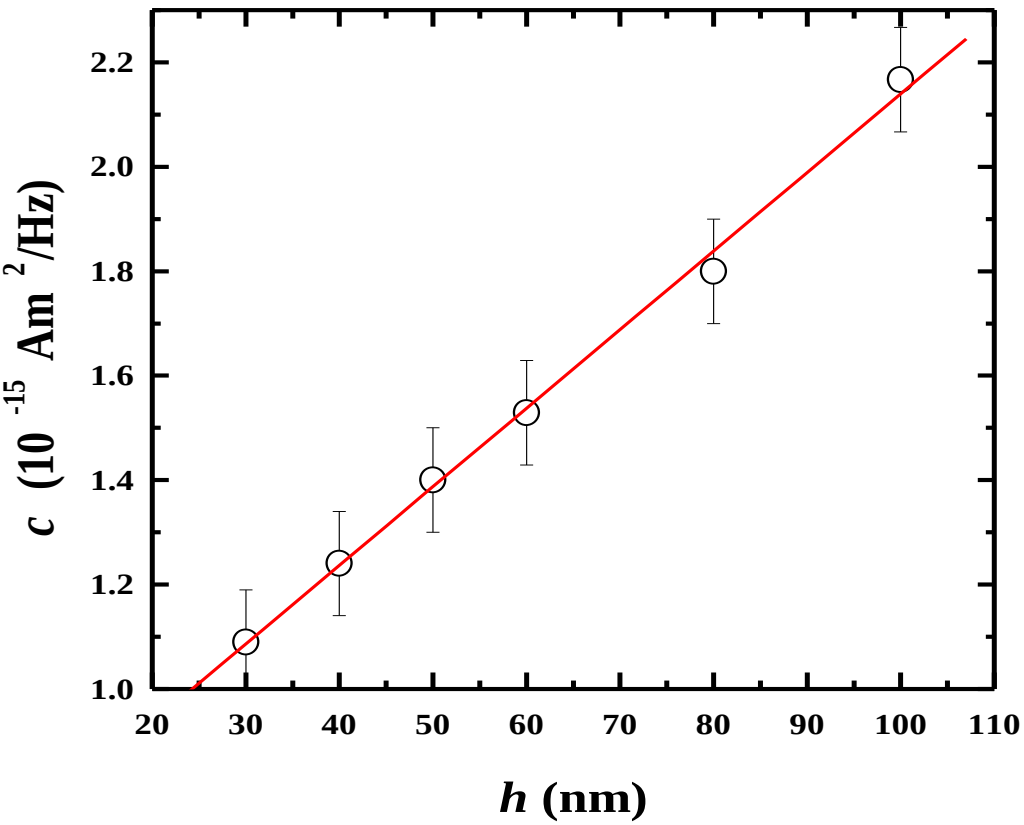

Figure 6.

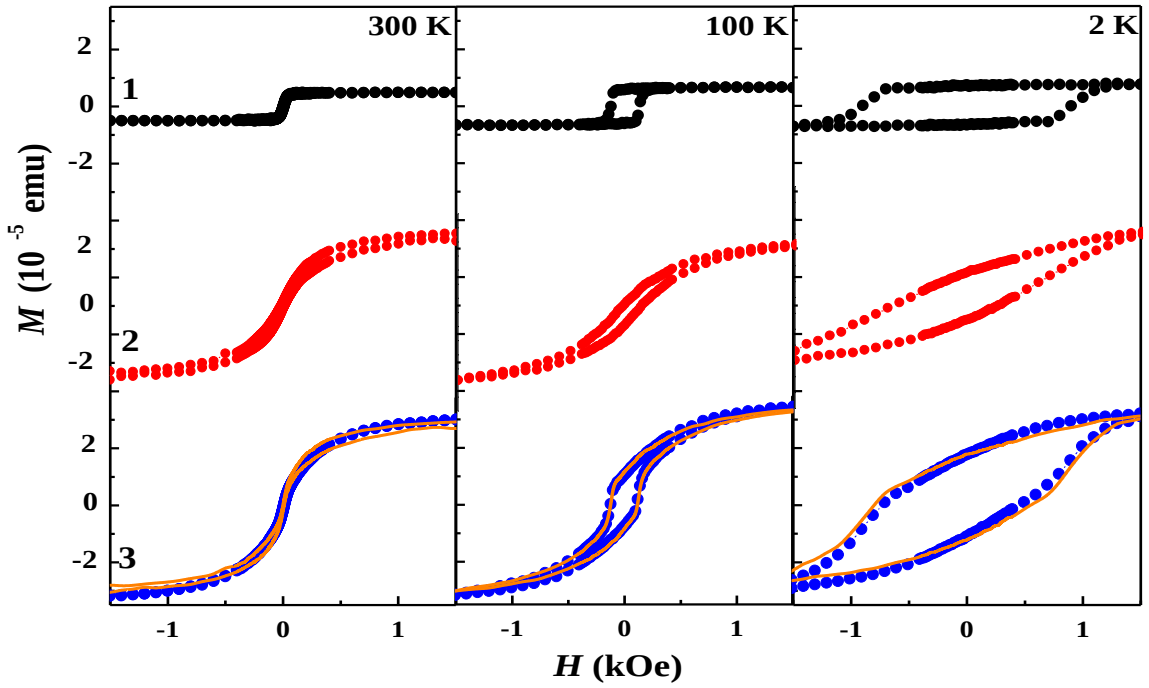

a)

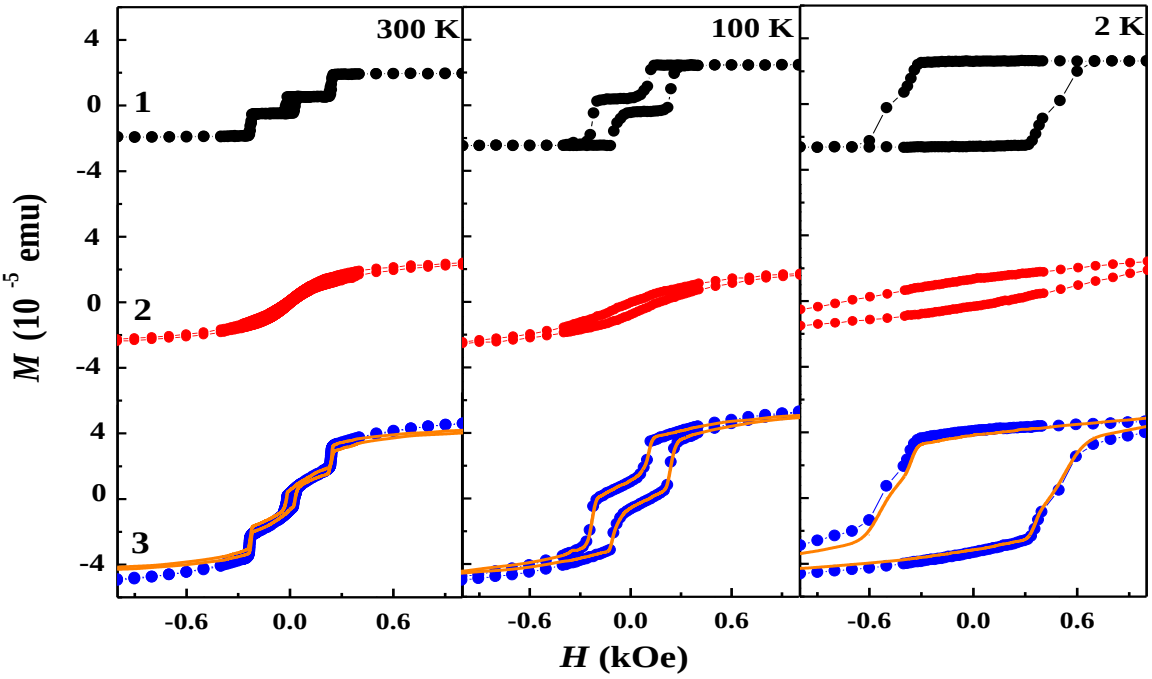

b)

Figure 7.

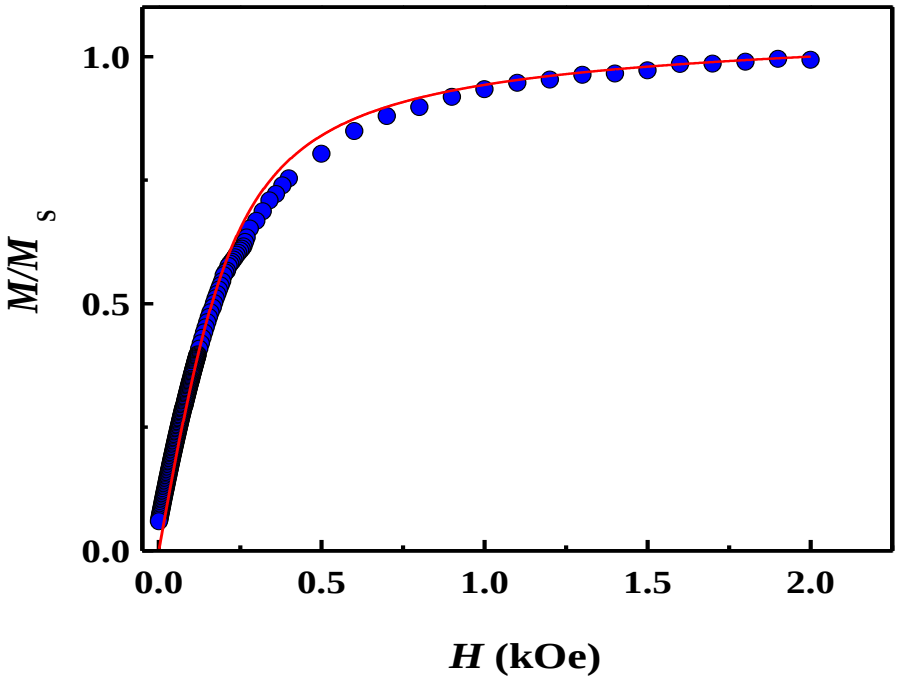

Figure 8.

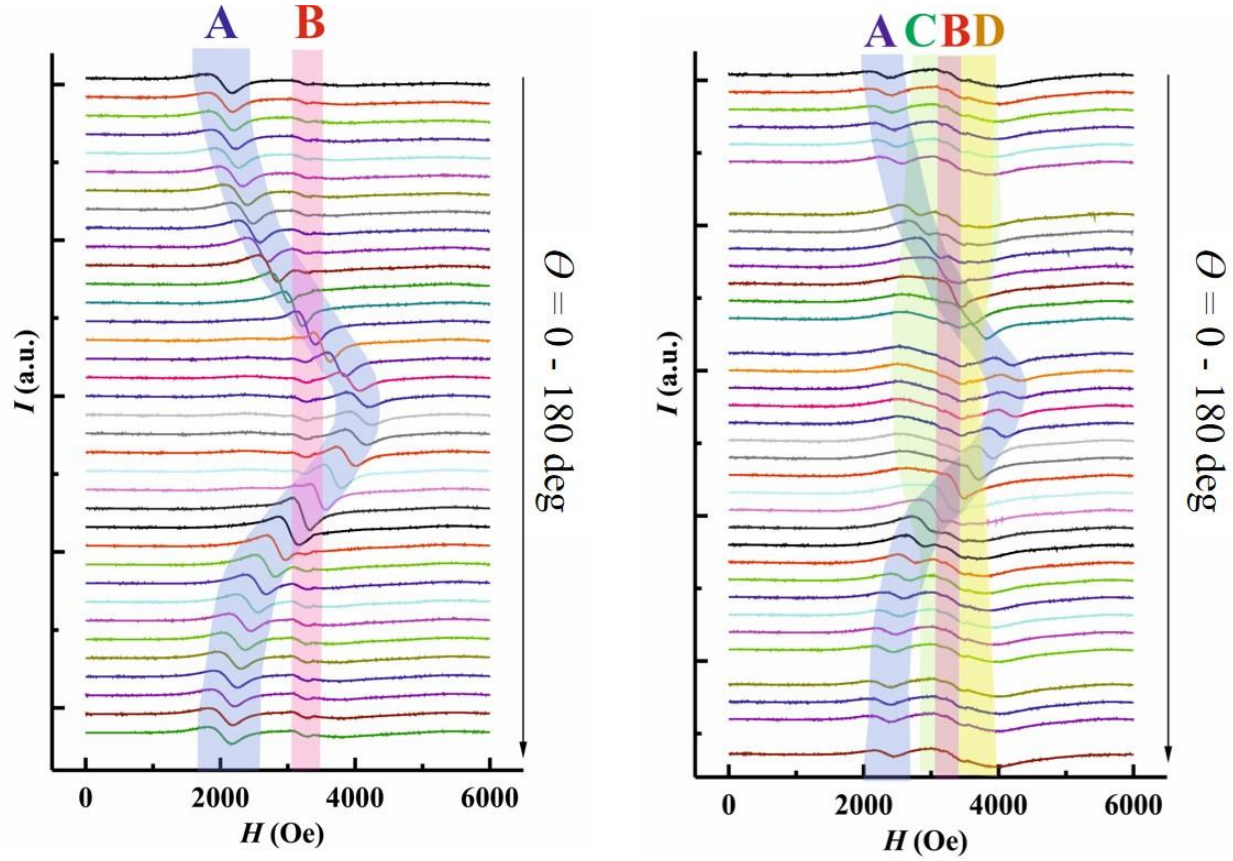
A
B
I (a.u.)
0
2000
4000
6000
H (Oe)
θ = 0 - 180 deg
A C B D
I (a.u.)
0
2000
4000
6000
H (Oe)
θ = 0 - 180 deg

a) b)

Figure 9.

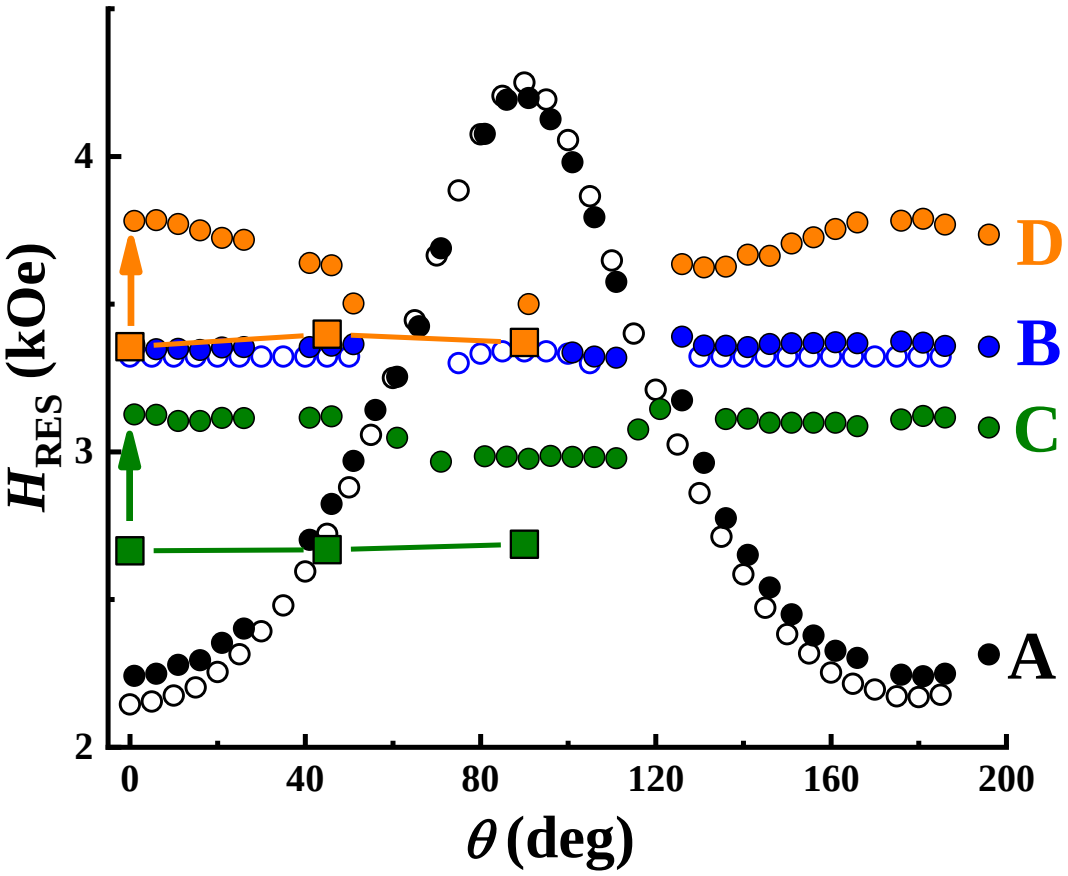

Figure 10.

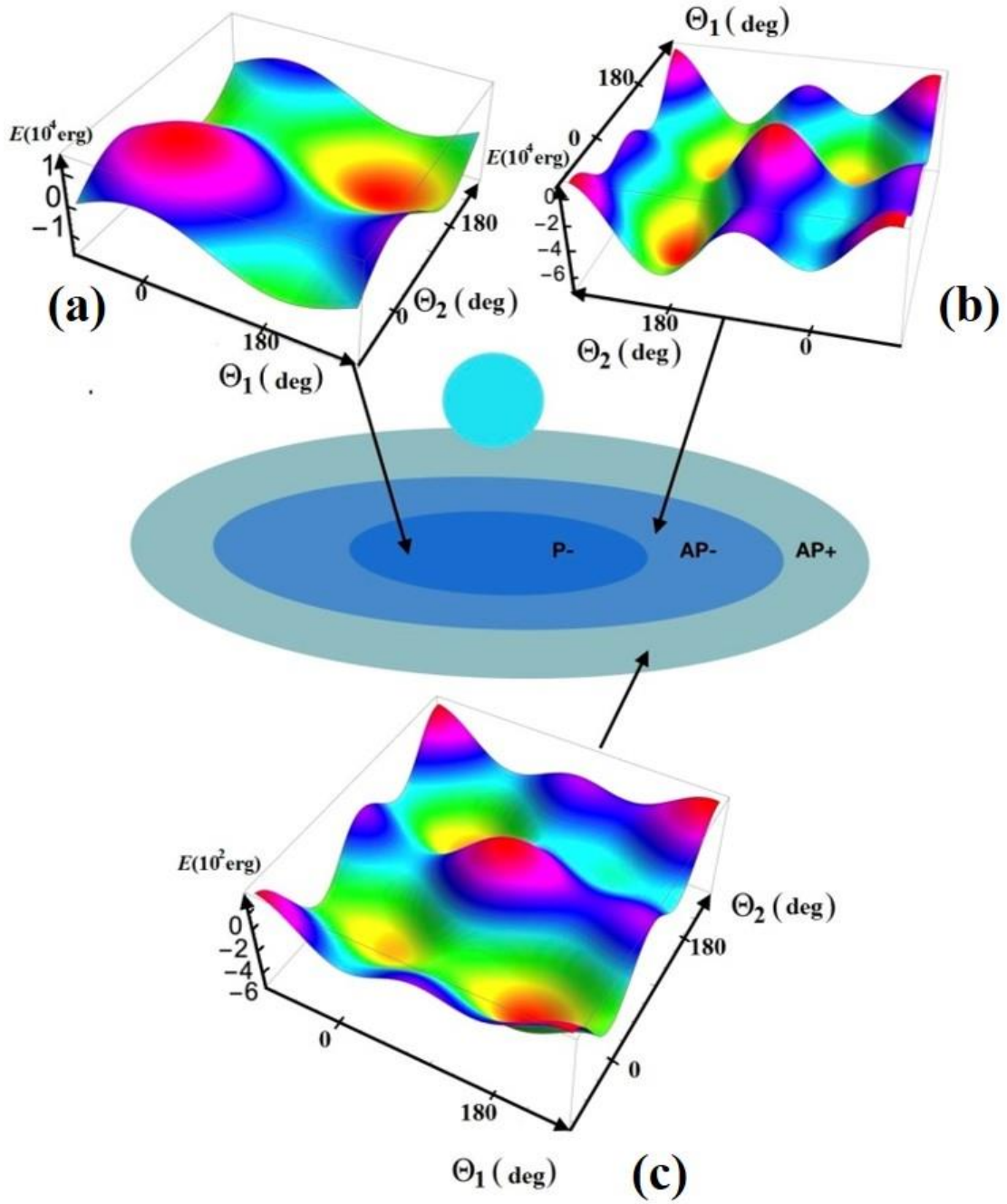
E(10^4 erg)
1
0
−1
0
180
Θ1 (deg)
0
180
Θ2 (deg)
(a)
Θ1 (deg)
180
0
E(10^4 erg)
0
−2
−4
−6
180
Θ2 (deg)
0
(b)
P-
AP-
AP+
E(10^2 erg)
0
−2
−4
−6
0
180
Θ1 (deg)
Θ2 (deg)
180
0
(c)

Figure 11.

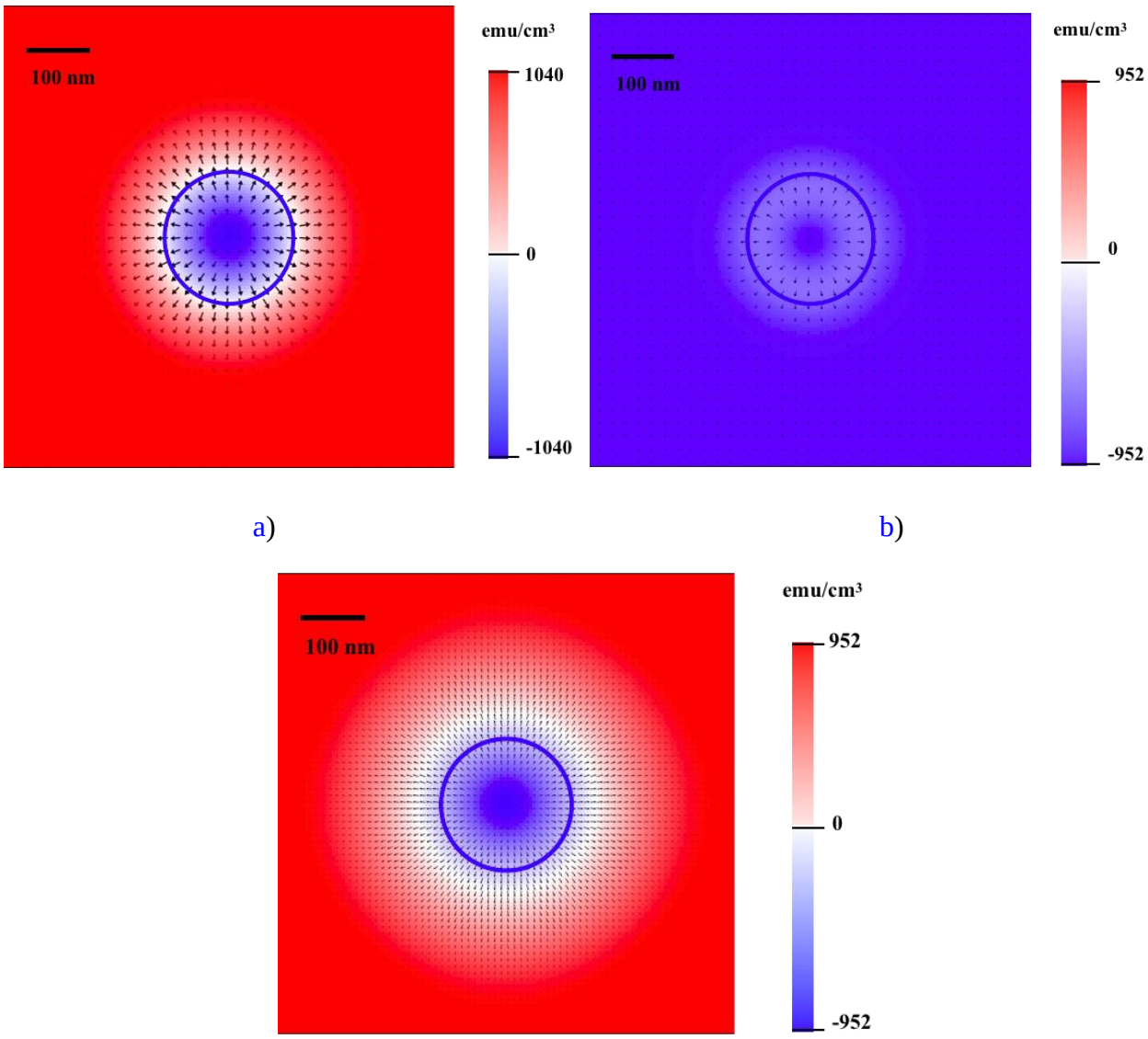

a) b)

c)

Figure 12.